



## Basins of Convergence in the Collinear Restricted Four-body Problem with a Repulsive Manev Potential

<sup>1,\*</sup>Euaggelos E. Zotos, <sup>2</sup>Md Sanam Suraj, <sup>2</sup>Rajiv Aggarwal and <sup>3</sup>Charanpreet Kaur

<sup>1</sup>Department of Physics  
School of Science  
Aristotle University of Thessaloniki  
GR-541 24, Thessaloniki, Greece  
[evzotos@physics.auth.gr](mailto:evzotos@physics.auth.gr)

<sup>2</sup>Department of Mathematics  
Sri Aurobindo College  
University of Delhi  
Delhi, India

<sup>3</sup>Department of Mathematics  
SGTB Khalsa College  
University of Delhi, North Campus  
New Delhi, India

\*Corresponding author

Received: March 1, 2020; Accepted: April 5, 2020

### Abstract

The Newton-Raphson basins of convergence, related to the equilibrium points, in the collinear restricted four-body problem with repulsive Manev potential are numerically investigated. We monitor the parametric evolution of the position as well as of the stability of the equilibrium points, as a function of the parameter  $e$ . The multivariate Newton-Raphson optimal method is used for revealing the basins of convergence, by classifying dense grids of initial conditions in several types of two-dimensional planes. We perform a systematic and thorough analysis in an attempt to understand how the parameter  $e$  affects the geometry as well as the basin entropy of the convergence regions. The convergence areas are related with the required number of iterations and also with the corresponding probability distributions.

**Keywords:** Restricted four-body problem; Basins of convergence; Fractal basin boundaries; Basin entropy

**MSC 2010 No.:** 65H04, 49M15, 65F10

## 1. Introduction

The dynamics of a system of  $N$ -bodies have captivated the interest of many researchers, scientists, and astronomers. Surely, one of the most intriguing models in celestial dynamics and mechanics is the problem of four bodies, where the fourth body is massless and therefore it does not affect the motion of the three primaries, in any way.

One of the many cases of the general collinear  $N$ -body configurations, studied in Moulton (1910), is the collinear four-body central configuration, where  $N$ -masses are arranged in a straight line. Moulton investigated one half of the  $N$  possible classes of different collinear configurations of  $N$ -particles. He found that in the problem with four equal masses there exist twelve collinear solutions, which are also referred to as Moulton solutions.

In the following years, Manev (Manev (1924); Manev (1925); Manev (1930a); Manev (1930b)) has also worked in the central force problem, by introducing a potential of the form  $A/r + B/r^2$ . Moreover, Mioc and Stoica (1997) discussed the same potential in the frame of the problem of two bodies. In the same vein, Alavi & Razmi (2015) used, for describing the evolution of disk galaxies, a similar correction term, with  $e > 0$ , which corresponds to a repulsive type of force.

Recently, Fakis & Kalvouridis (2013) explored the dynamical system of  $N$  bodies, where the primary located at the center creates a force field with the inverse cube correction term and revealed the various properties of the test particle. Furthermore, in Fakis & Kalvouridis (2014) they analyzed the curves of zero velocity and unveiled the various properties in the problem of  $N + 1$  bodies, using a quasi-homogeneous potential. Later on, the Copenhagen problem has been studied in Fakis & kalvouridis (2017), where they located the coordinates of the points of equilibrium and they determined the zero velocity surfaces.

A special case of the system of four bodies is the collinear restricted four-body problem. For this configuration of the primaries we should mention the following important works: The asymptotic solutions, as well as the stable and unstable manifolds associated to the Lyapunov periodic orbits, have been numerically investigated in Papadakis (2007). In Arribas et al. (2016a) they have investigated the case where the peripheral primaries are sources of radiation. In their study, they have illustrated the position and the stability of the libration points analytically, under the consideration that the radiation force is greater than the gravitational force. Similarly, in Arribas et al. (2016b) they extended their study by exploring the out-of-plane libration points, i.e., the libration points which exist outside the plane of the primaries. Whereas, in Barrabés et al. (2017) they have investigated the relative equilibria and their linear stability in the spatial collinear four-body configuration, with a Manev type potential. Moreover, in Suraj et al. (2018a) we have revealed the positions of the libration points and their stability when the mass of the infinitesimal body varies. Recently, the evolution of the families of symmetric periodic solutions and the evolution of the spiral points, which shows the connection between heteroclinic orbits and the equilibrium points were discussed in detail in Palacios et al. (2019). Finally, in Alvarez-Ramirez et al. (2019) they have computed the high order parameterizations of the stable/unstable manifolds, linked with the libration points, to allocate the orbits that eject from a quadruple collision, while they also analytically showed the

existence of ejection-direct escape orbits.

In the recent years, a plethora of papers has been devoted on the Newton-Raphson (NR) basins of convergence (BOC) in Hamiltonian systems, such as the generalized Hill problem (e.g. Zotos (2017d)), the problem of three bodies (e.g. Zotos (2016); Zotos (2017c)), of four bodies (e.g. Zotos (2017a); Zotos (2017b); Suraj et al. (2017)), and of five bodies (e.g. Suraj et al. (2019a); Zotos and Suraj (2017); Suraj et al. (2019b); Suraj et al. (2019c); Suraj et al. (2019d)), the Sitnikov three-body problem (e.g. Zotos et al. (2018b)), the Sitnikov four-body problem (e.g. Zotos et al. (2018a)), the pseudo-Newtonian Sitnikov problem (e.g. Zotos et al. (2018c)), the restricted pseudo-Newtonian four-body problem (e.g. Suraj et al. (2019e)), and the Copenhagen system with a potential of Manev-type (e.g. Suraj et al. (2018b)). The study of the BOC is a very important aspect since they allow us to know the optimal starting points for an iterative scheme for providing the coordinates of the points of equilibrium, which in many cases, cannot be determined analytically.

In the present work, we will adopt the same numerical methods, used in the above-mentioned papers, for determining the convergence dynamics of the collinear restricted four-body system with potential of Manev-type. At this point, we should emphasize that the points of equilibrium of this, along with the respective basins of convergence, have not been studied before. On this basis, we perform a novel investigation in a very interesting system and therefore all the presented outcomes are new and advance our existing knowledge on the field of the  $N$  body problem.

In Section 2 we provide the mathematical description of the dynamical model, while in Section 3 we present the evolution of the coordinates and the linear stability of the points of equilibrium. In the following Section we illustrate the geometry along with the basic properties of the NR BOC. In the final Section 5 we provide the discussion of our work.

## 2. Properties of the dynamical system

We consider the scenario according to which an infinitesimal mass  $m$  moves around three primary bodies  $P_0$ ,  $P_1$ , and  $P_2$ , with point masses  $m_0$ ,  $m_1$ , and  $m_2$ , respectively. Furthermore, we assume that  $m_1 = m_2$ . In particular, the central primary  $P_0$  is located between the primaries  $P_1$  and  $P_2$  (see Figure 1). The mass of  $P_0$  is  $m_0 = \beta m_1 = \beta m_2$ , where  $\beta$  is the so-called mass parameter.

In our case the attraction of the peripheral bodies is according to the classical Newtonian potential  $-1/r$ , while on the other hand the gravitational attraction, due to the central body  $P_0$ , is described by a potential form  $-1/r + e/r^2$ , where  $e > 0$  is an arbitrary parameter which determines the strength of the Manev-type force (Manev (1924); Manev (1925)).

Moreover, the system of units is chosen in such a way so that the distance between the two peripheral bodies is one ( $\|P_1P_2\| = 1$ ), while also  $Gm_1 = Gm_2 = 1$ , where of course  $G$  is the constant of gravity. Therefore, the coordinates of the three primary bodies are:  $P_0(0, 0, 0)$ ,  $P_1(-x_p, 0, 0)$ , and  $P_2(x_p, 0, 0)$ , where  $x_p = 1/2$ .

According to Barrabés et al. (2017) the peripheral bodies can perform circular orbits (where the

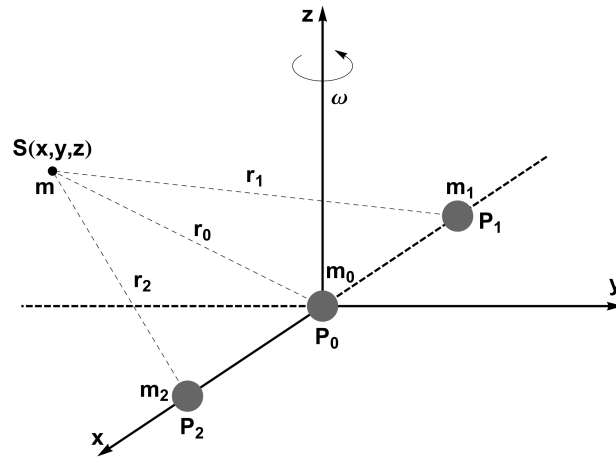


Figure 1. The planar configuration of the three primaries in collinear configuration

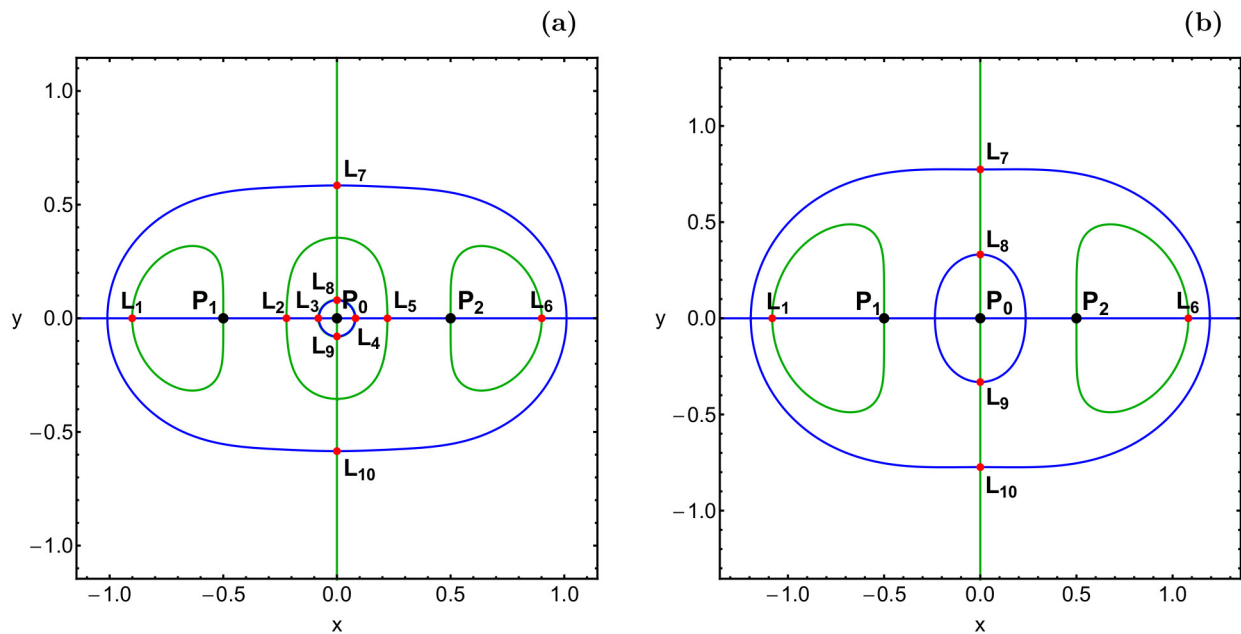


Figure 2. The intersections of the contours of the equations  $\Omega_x = 0$  (green) and  $\Omega_y = 0$  (blue) pinpoint the locations (red dots) of the points of equilibrium ( $L_i, i = 1, 10$ ). (a):  $e = 0.04$  and (b):  $e = 0.2$ . The centers of the two primaries ( $P_i, i = 1, 2$ ) are indicated using black dots. (Color figure online)

angular velocity  $\omega$  is constant) if and only if  $\omega = \Delta$ , with

$$\Delta = 2(1 + 4\beta - 16e\beta) > 0. \tag{1}$$

For having  $\Delta > 0$  the rule, regarding the permissible values of  $e$ , reads

$$e < \frac{1 + 4\beta}{16\beta}, \tag{2}$$

for fixed  $\beta > 0$ .

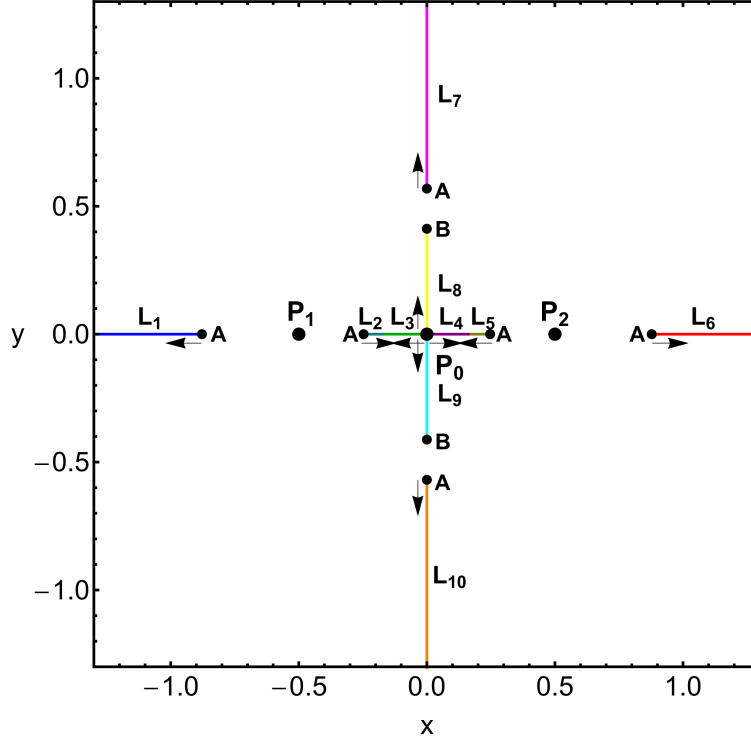


**Figure 3.** The evolution on the configuration space  $(x, y)$  of the coordinates of the points of equilibrium of the system, when  $e \in (0, 0.3125)$ . The small arrows indicate how the libration points move, as the value of  $e$  increases. The centers of the primaries are shown by big black dots, while points A and B (small black dots) correspond to  $e = 0$  and  $e \rightarrow 0.3125$ , respectively. (Color figure online)

The negative effective potential is given by

$$\Omega(x, y, z) = \frac{1}{\Delta} \left[ \sum_{i=1}^2 \frac{1}{r_i} + \beta \left( \frac{1}{r_0} - \frac{e}{r_0^2} \right) \right] + \frac{1}{2} (x^2 + y^2), \quad (3)$$

where

$$\begin{aligned} r_0(x, y, z) &= \sqrt{(x^2 + y^2 + z^2)}, \\ r_1(x, y, z) &= \sqrt{(x - x_p)^2 + y^2 + z^2}, \\ r_2(x, y, z) &= \sqrt{(x + x_p)^2 + y^2 + z^2}. \end{aligned} \quad (4)$$

The spatial motion of the massless body is governed by the set of equations

$$\begin{aligned} \ddot{x} - 2\dot{y} &= \Omega_x = \frac{\partial \Omega}{\partial x}, \\ \ddot{y} + 2\dot{x} &= \Omega_y = \frac{\partial \Omega}{\partial y}, \\ \ddot{z} &= \Omega_z = \frac{\partial \Omega}{\partial z}, \end{aligned} \quad (5)$$

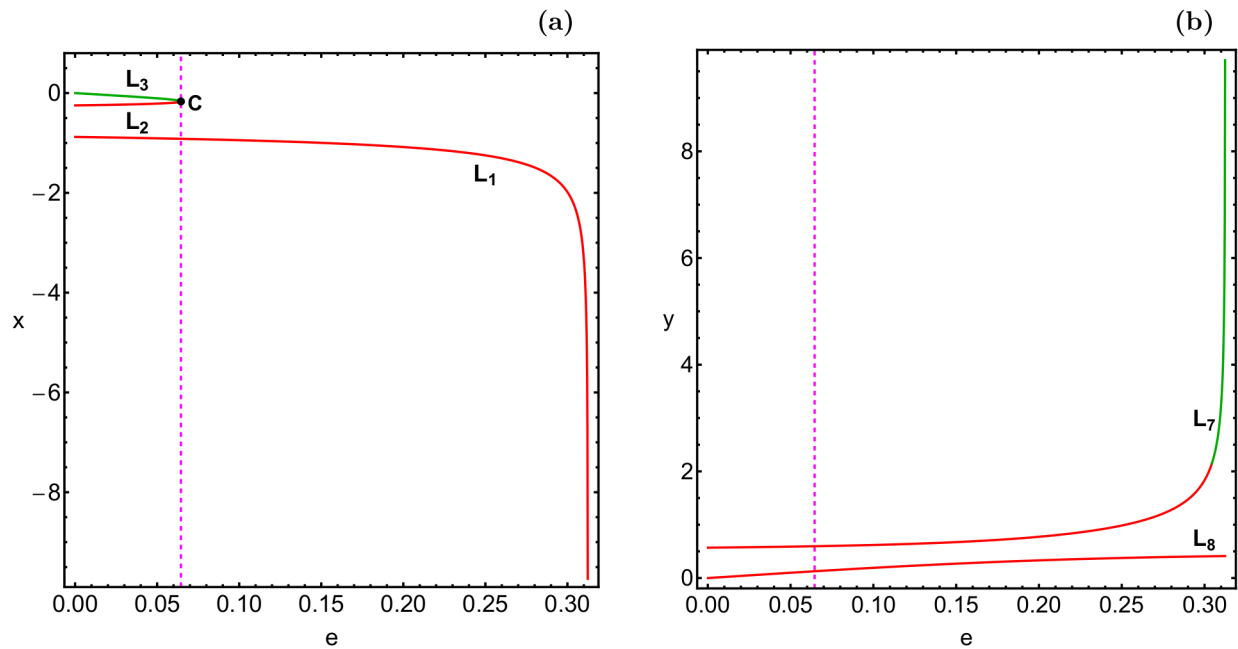


**Figure 4.** Parametric evolution of the linear stability (green) and instability (red) of the points of equilibrium located on the (a-left): negative  $x$  axis ( $L_1, L_2, L_3$ ) and (b-right): positive  $y$  axis ( $L_7, L_8$ ). The dashed vertical magenta line denotes the position of the critical value  $e^*$ . The point C indicates the position where  $L_2$  and  $L_3$  collide with each other, when  $e = e^*$ . (Color figure online)

where

$$\begin{aligned} \Omega_x(x, y) &= \frac{1}{\Delta} \left[ -\frac{x_1}{r_1^3} - \frac{x_2}{r_2^3} + \beta \left( -\frac{x}{r_0^3} + \frac{2ex}{r_0^4} \right) \right] + x, \\ \Omega_y(x, y) &= \frac{1}{\Delta} \left[ -\frac{y}{r_1^3} - \frac{y}{r_2^3} + \beta \left( -\frac{y}{r_0^3} + \frac{2ey}{r_0^4} \right) \right] + y, \end{aligned} \quad (6)$$

with  $x_1 = x - x_p$  and  $x_2 = x + x_p$ .

### 3. Equilibrium Points

In a Hamiltonian system an equilibrium point is valid if and only if the first and second order derivatives of the coordinates are all equal to zero. On this basis, for obtaining the coordinates  $(x_0, y_0, z_0)$  of the points of equilibrium all we have to do is to solve the system

$$\Omega_x = \Omega_y = \Omega_z = 0. \quad (7)$$

At this point, it should be emphasized that the above system of equations does not have analytical solutions in closed form, which automatically means that the coordinates of the libration point of the system can be derived only by using numerical methods.

Our analysis will be restricted only to the coplanar (when  $z = \dot{z} = 0$ ) points of equilibrium on the configuration space  $(x, y)$ . Additionally, we will consider the case with  $\beta = 1$ , which implies that we have equally massed primaries ( $m_0 = m_1 = m_2$ ). This means that the value of  $e$  lies in the interval  $(0, 0.3125)$ .

The parameter  $e$  determines the total number of points of equilibrium of the system. More precisely, our computations suggest that:

- When  $e \in (0, 0.06464946]$  the dynamical system has ten points of equilibrium (see part (a) of Figure 2).
- When  $e \in (0.06464946, 0.3125)$  the dynamical system has six points of equilibrium (see part (b) of Figure 2).

The value  $e^* = 0.06464946$  a critical level of  $e$ , as it corresponds to the threshold value where the total number of the points of equilibrium changes.

The positions of the coordinates of the libration points on the plane  $(x, y)$  correspond to the intersections of  $\Omega_x = 0$  and  $\Omega_y = 0$ . In Figure 2(a-b) we present the locations of the points of equilibrium, when (a):  $e = 0.04$  and (b):  $e = 0.2$ . The numbering  $L_i$ ,  $i = 1, \dots, 10$ , of the libration points is also explained in the same figure.

The evolution of the coordinates of the points of equilibrium, as a function of  $e$ , when  $e \in (0, 0.3125)$  is given in Figure 3. We see that as soon as  $e$  is just above zero two pairs of libration points appear from the center of the primary  $P_0$ . Two of them,  $L_3$  and  $L_4$  lie on the  $x$  axis, while the  $L_8$  and  $L_9$ , lie on the  $y$  axis. It is seen that as the value of  $e$  increases the points  $L_3$  and  $L_4$  move on collision course with  $L_2$  and  $L_5$ , respectively. This collision occurs exactly at the critical value  $e^*$  and all these points of equilibrium are mutually annihilated. At the same time, all the other libration points continue to move away from the primary bodies. It is interesting to note that all the points of equilibrium evolve along the axes  $x = 0$  and  $y = 0$ .

There is no doubt that apart from the positions of the points of equilibrium one should also be aware of their linear stability. For obtaining the linear stability of the points of equilibrium we computed the corresponding four roots of the characteristic equation, by following the numerical method explained in detail in Zotos (2017c). Our computations suggest that when  $e \in (0, 0.3125)$ ,

- The equilibrium points  $L_1, L_2, L_5, L_6, L_8$ , and  $L_9$  are always linearly unstable.
- The equilibrium points  $L_3$  and  $L_4$  are always linearly stable.
- The equilibrium points  $L_7$  and  $L_{10}$  are linearly stable when  $0 < e \leq 0.30443155$ , while when  $0.30443155 < e < 0.3125$  they become linearly stable.

In parts (a) and (b) of Figure 4, we show the evolution of the linear stability (green) and instability (red) of the points of equilibrium  $L_1, L_2, L_3, L_7$ , and  $L_8$ . The evolution of the rest of the points is mirror symmetrical.

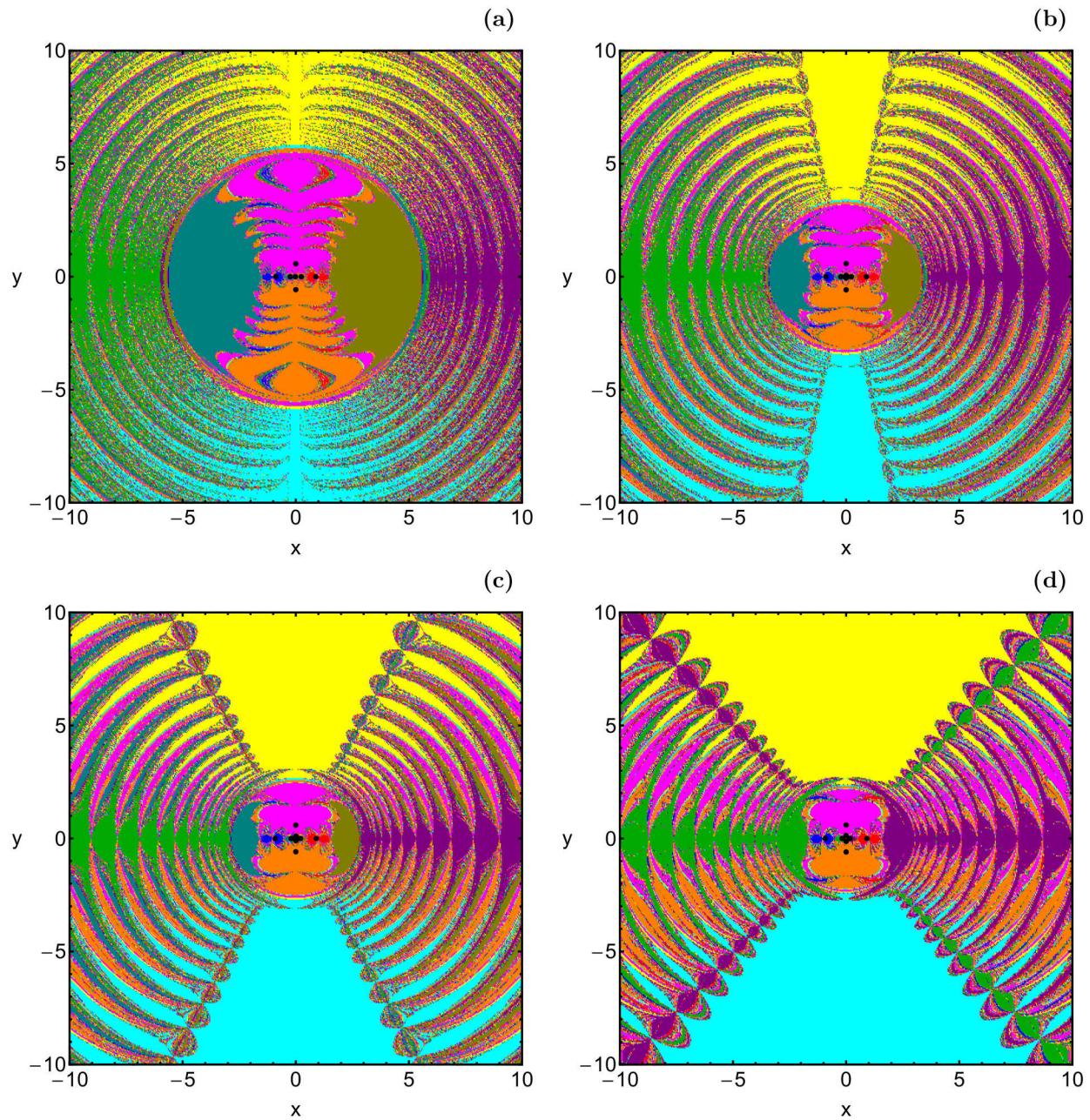


**Figure 5.** The NR BOC on the plane  $(x, y)$ , for the first case, where ten points of equilibrium are present. (a):  $e = 0.01$ ; (b):  $e = 0.03$ ; (c):  $e = 0.05$ ; (d):  $e = 0.064649$ . Black dots pinpoint the points of equilibrium. The colors denoting the 10 numerical attractors (libration points) are as follows:  $L_1$  (blue);  $L_2$  (teal);  $L_3$  (green);  $L_4$  (purple);  $L_5$  (olive);  $L_6$  (red);  $L_7$  (magenta);  $L_8$  (yellow);  $L_9$  (cyan);  $L_{10}$  (orange); points which do not converge (white). (Color figure online)

#### 4. The Newton-Raphson Convergence Basins

In this section, we will present the shapes and features of the BOC on the plane  $(x, y)$ , for several characteristic values of  $e$ . For solving the system of Equations (7) we use the following Newton-

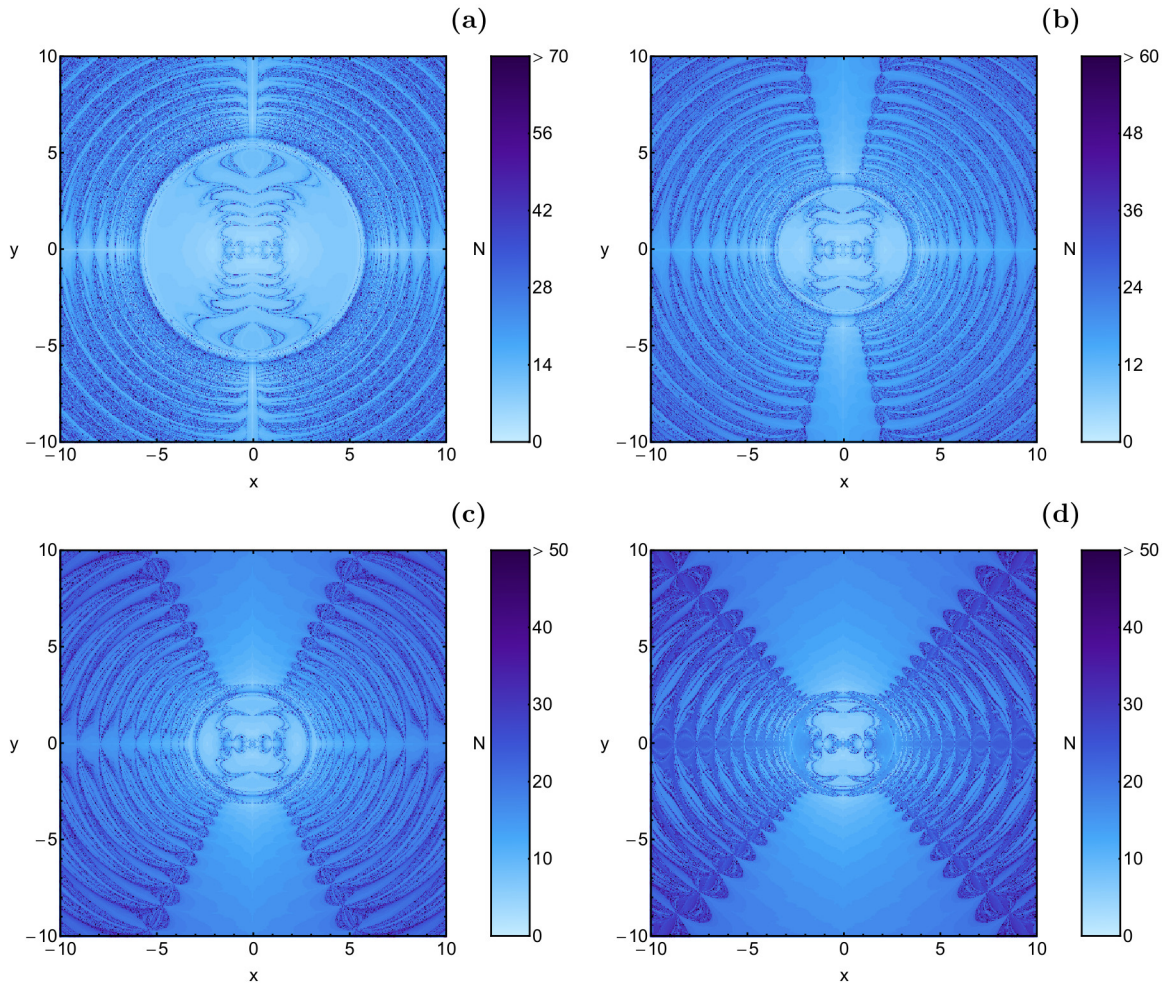


**Figure 6.** The corresponding required numbers of iterations for the first case. (Color figure online)

Raphson (NR) iterative scheme,

$$\begin{aligned}
 x_{n+1} &= x_n - \left( \frac{\Omega_x \Omega_{yy} - \Omega_y \Omega_{xy}}{\Omega_{yy} \Omega_{xx} - \Omega_{xy}^2} \right)_{(x_n, y_n)}, \\
 y_{n+1} &= y_n + \left( \frac{\Omega_x \Omega_{yx} - \Omega_y \Omega_{xx}}{\Omega_{yy} \Omega_{xx} - \Omega_{xy}^2} \right)_{(x_n, y_n)},
 \end{aligned} \tag{8}$$

while all the details of how the numerical procedure of obtaining the BOC works are described in Section 4 of Zotos (2017c).

In the following for visualizing the BOC on the configuration space  $(x, y)$  we will deploy two-dimensional diagrams with a color code. In these plots, each point (initial condition) receives a color that corresponds to the respective numerical attractor (point of equilibrium), thus following the pioneer graphical approach introduced and used in Nagler (2004) and Nagler (2005).

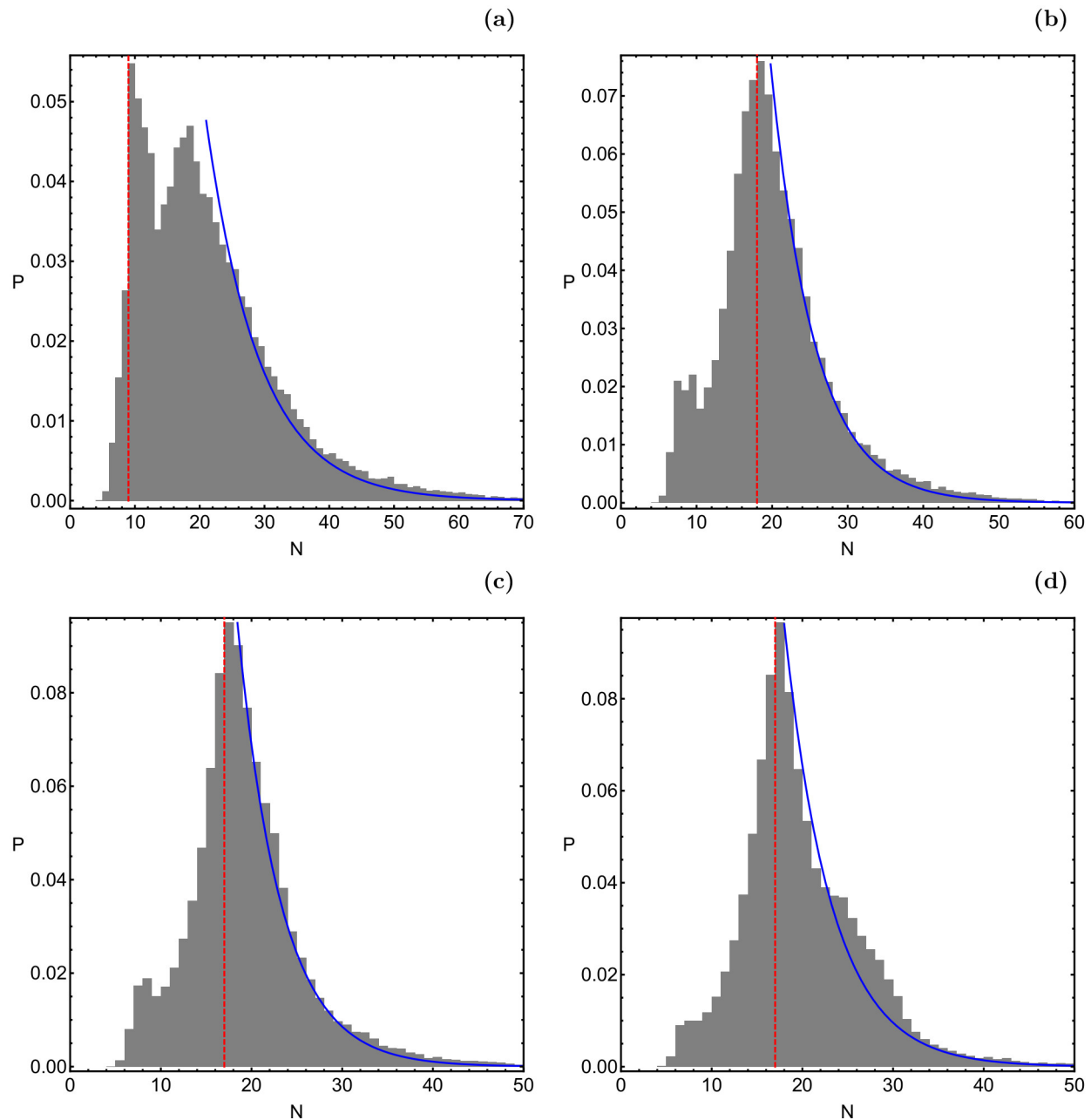


**Figure 7.** Probability histograms for the first case. The red dashed vertical line indicates  $N^*$ . (Color figure online)

#### 4.1. Case I: Ten equilibrium points

We start with  $0 < e < e^*$ , when ten points of equilibrium exist. In Figure 5(a-d) we present, for four values of  $e$ , the evolution of the NR BOC. We observe that the plane  $(x, y)$  is always covered by a plethora of well-defined BOC, which all extend to infinity. However, we can also distinguish several local areas (e.g., near the basin boundaries), where a highly fractal mixture of starting points exist. In the next section we will present quantitative arguments, regarding the fractal degree of the configuration plane, as in Aguirre et al. (2001) and Aguirre et al. (2009). The geometry of the BOC on the plane  $(x, y)$ , is mainly composed of two shapes: (i) the central region, occupied by BOC

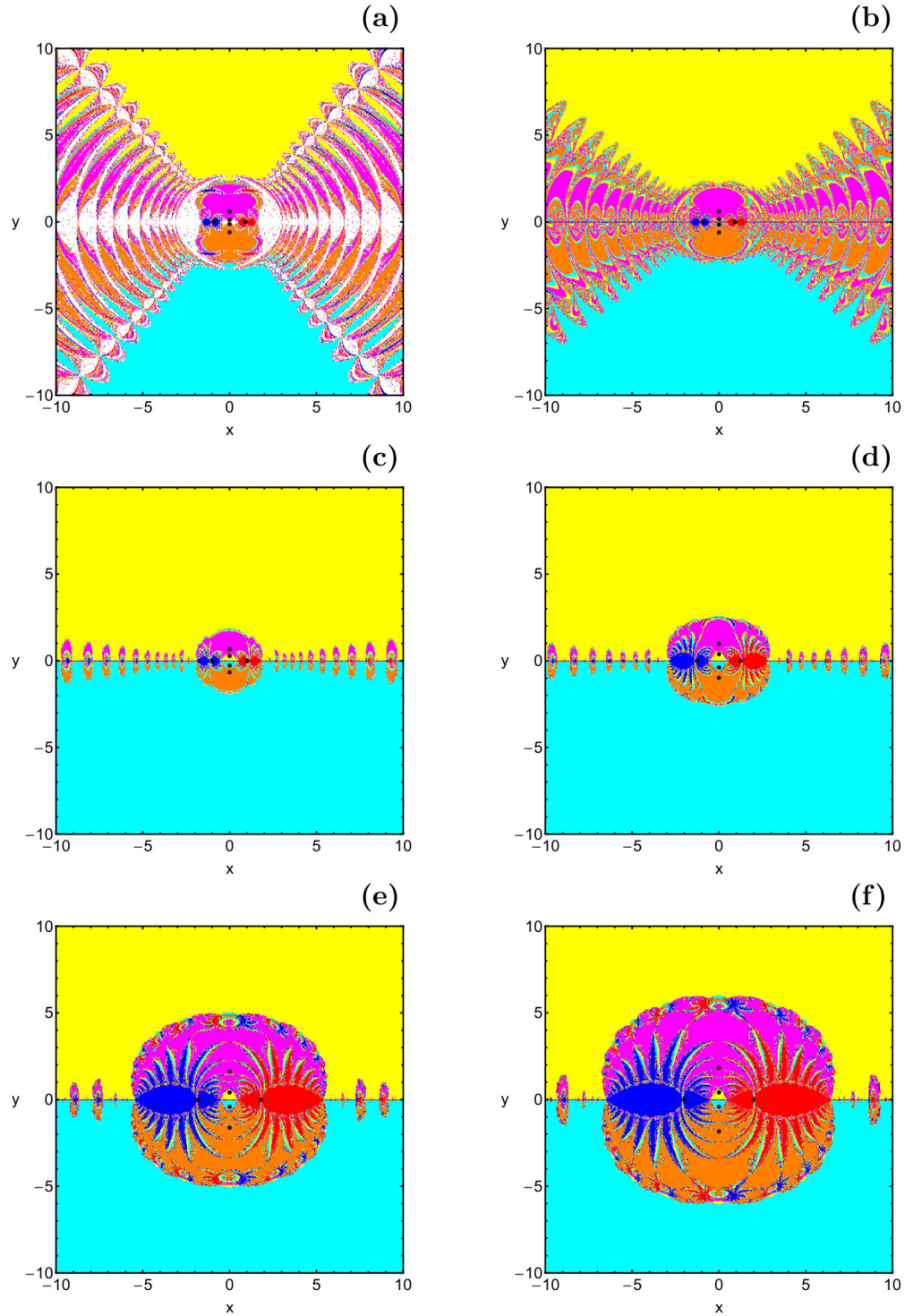


**Figure 8.** The NR BOC on the plane  $(x, y)$  for the second case, where six points of equilibrium are present. (a):  $e = 0.06465$ ; (b):  $e = 0.08$ ; (c):  $e = 0.15$ ; (d):  $e = 0.25$ ; (e):  $e = 0.295$ ; (f):  $e = 0.30$ . Black dots pinpoint the points of equilibrium. The colors denoting the 6 numerical attractors (libration points) are as in Figure 5. (Color figure online)

and (ii) the exterior region, where the BOC has the shape of wings.

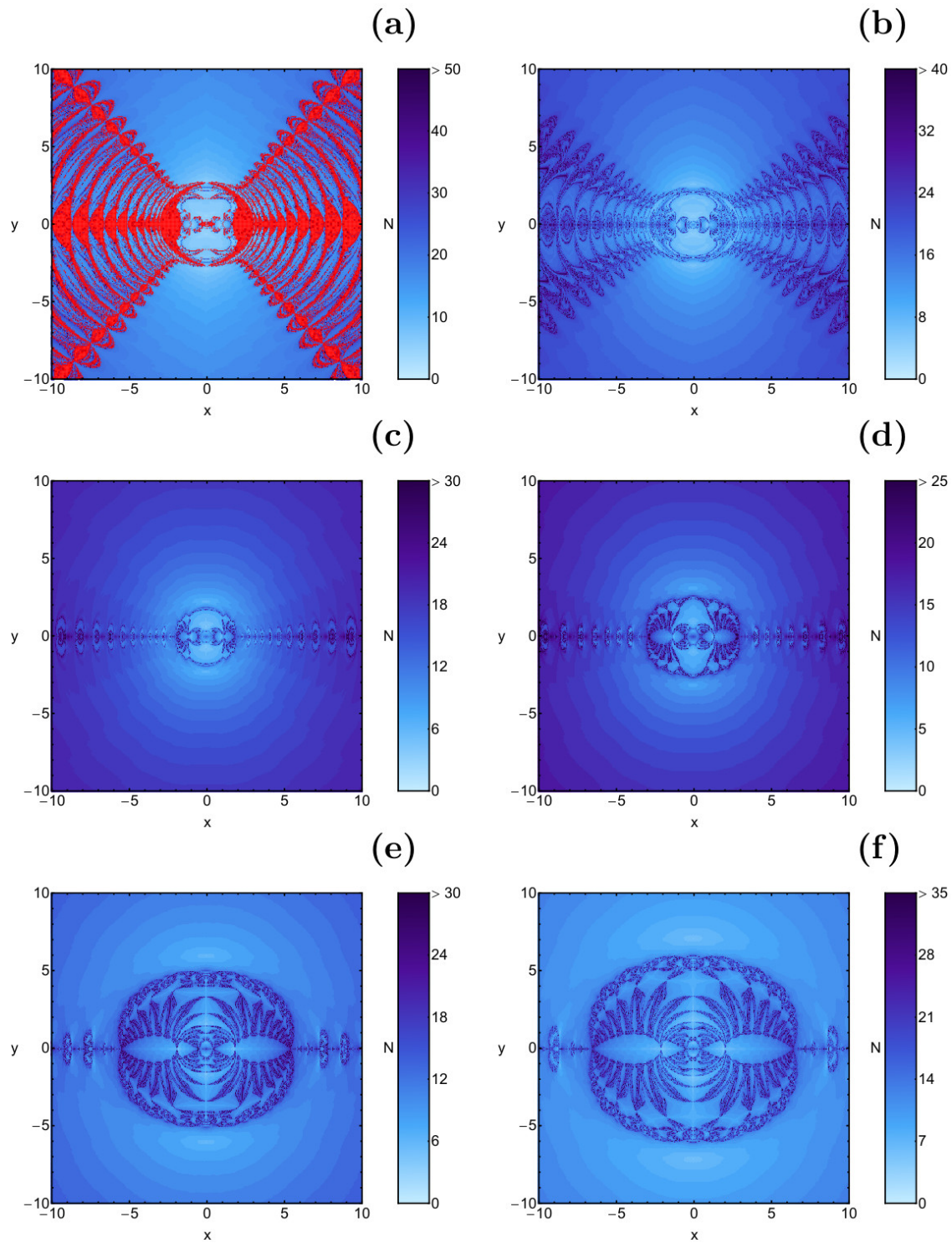


**Figure 9.** The corresponding required numbers of iterations for the second case. Red color denotes the points which do not converge. (Color figure online)

As the value of  $e$  grows the geometry of the plane  $(x, y)$  drastically changes, as follows:

- The area of the central circular region (corresponding to points of equilibrium  $L_1, L_2, L_5, L_6, L_7$ ,

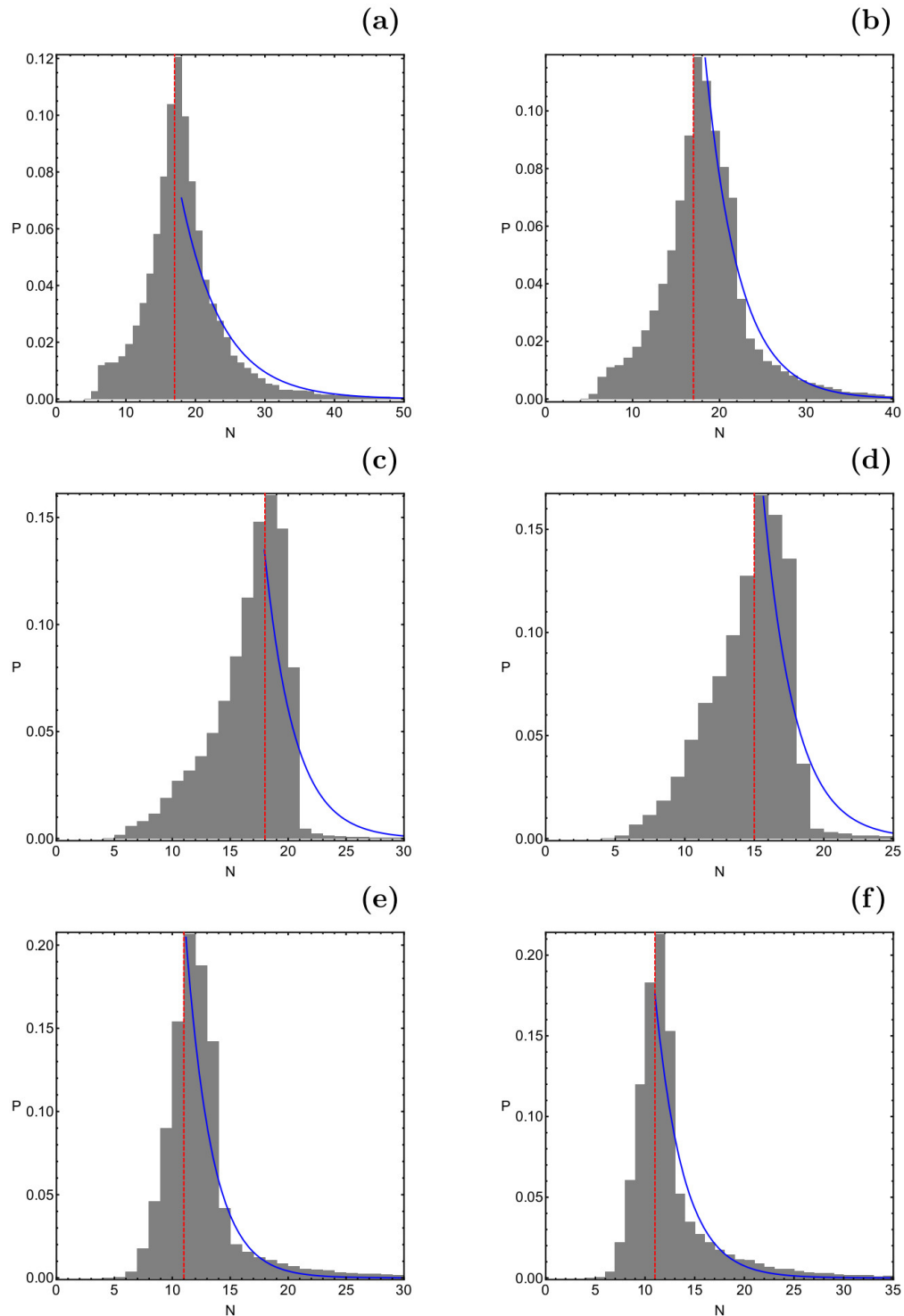


**Figure 10.** Probability histograms for the second case. The red dashed vertical line indicates  $N^*$ . (Color figure online)

and  $L_{10}$ ) decreases.

- The extent of the wing-shape structures in the exterior region is reduced. In particular, these structures tend to the horizontal axis.
- The area of the BOC in the exterior region, corresponding to points  $L_8$  and  $L_9$  increases, while at

the same time their boundaries become less chaotic (fractal).

The distributions of the iterations  $N$ , required for the desired accuracy (of 15 decimal digits regarding the coordinates of the points of equilibrium), are given in Figure 6(a-d), using tones of blue. Inspecting the accompanying colorbar of the diagrams one can observe that the average value of the required iterations is reduced with an increasing value of  $e$ . In Figure 7(a-d) we provide the probability histograms.

In all diagrams, the histograms are extended so much as to cover 95% of the distributions, while  $N^*$  is the most probable number of iterations. For all four studied cases, the geometry of the histograms follows the typical shape, according to which there is a global maximum, while the probability is reduced from both sides of the global peak.

## 4.2. Case II: Six equilibrium points

When  $e^* < e < 0.3125$  there exist six points of equilibrium: two on the horizontal  $x$  axis and four on the vertical  $y$  axis. The evolution of the NR BOC, for six values of  $e$ , is illustrated in Figure 8(a-f). With increasing value of  $e$  the following phenomena occur on the plane  $(x, y)$ :

- The wing-shape structures continue to come closer to the horizontal axis and eventually they vanish.
- The area of the central region decreases in the interval  $e^* < e < 0.18$ , while for higher values of  $e$  its size grows significantly.
- The structure of the BOC, corresponding to points  $L_8$  and  $L_9$  seems to be unaffected. In fact, these basins dominate the exterior region.

In part (a) of Figure 8, where  $e = 0.06465$ , that is a value just above the critical value  $e^*$ , we identified a significant amount of starting points which do not converge to any of the numerical attractors. Therefore, the natural question that arises is: are these nodes true non-converging initial conditions? To answer this question we conducted additional numerical calculations, while the maximum number  $N$  of iterations was increased to  $N = 50000$ . It was found that all these nodes are in reality very slow converging starting conditions. Specifically, all of them eventually do converge to one of the collinear points of equilibrium  $L_1$  or  $L_6$ , however only after a huge number of iteration, which in many cases exceeds  $N = 10^5$ .

The appearance of slow converging points near the critical value of the system can be explained as follows: Let us consider a Poincaré map in which we look for fixed points. The map is called  $f$  and let  $x$  be a point of the domain of the map. And the application of the map is  $x_{n+1} = f(x_n)$ . So, we are looking for a point  $x_0$  with the property  $f(x_0) = x_0$ . We can also define the map  $g(x) = f(x) - x$ . Then any fixed point of  $f$  is a zero point of  $g$ . Therefore, the problem consists of finding a zero point of a function and for this problem we have the well known Newton-Raphson method. As long as the fixed point  $x_0$  is not degenerate, this method works well and is reliable. However,

the method runs into trouble, if the point  $x_0$  becomes degenerate, as it happens for example when the point  $x_0$  runs into a bifurcation (we can think of a bifurcation of the periodic orbit in the flow which corresponds to the fixed point  $x_0$  of the Poincaré map).

The reason for the trouble lies in the intrinsic properties of the numerical method. In particular, in each step of the NR method we have to construct the inverse matrix of the matrix  $D_g$ , i.e. of the matrix of the partial derivatives of  $g$  taken at the actual point  $x$  of the present step of the Newton-Raphson method. And note that  $D_g = D_f - 1$ , where 1 is here the unitary matrix. As long as  $D_g$  does not have any eigenvalue 0, this inverse matrix is nonsingular and exists. However, exactly at the bifurcations of the point  $x_0$   $D_f$  acquires an eigenvalue 1 and the rank of  $D_g$  drops and we can no longer construct the inverse matrix to  $D_g$ . Numerically, the intent of this construction diverges and the whole Newton-Raphson method fails. Therefore, the method can not be used to search for a fixed point which is just in the process of a bifurcation. Remember that at saddle-center bifurcations or pitchfork bifurcations of periodic orbits an eigenvalue of the orbit (eigenvalue of  $D_f$ ) runs through 1.

Also, in the case of a parameter value (the parameter  $e$  in our case) near such a bifurcation, we come into numerical problems. Then an eigenvalue of  $D_f$  is close to 1, an eigenvalue of  $D_g$  is close to zero and the numerical construction of the inverse of  $D_g$  is highly unstable. Usually, in such a case the Newton-Raphson method exhibits an extremely slow convergence or it does not converge at all, by jumping irregularly around random values. Obviously, as we move away from the critical values of the system the amount of slow or not converging points is drastically reduced.

The distributions of  $N$  are presented in Figure 9(a-f), while the corresponding probability histograms are shown in Figure 10(a-f). From the histograms of Figure 9 it is evident that the value of  $N^*$  is reduced, with an increasing value of  $e$ .

### 4.3. Additional information

Through the basin diagrams on the plane  $(x, y)$  (see Figures 5 and 8) we can extract valuable information on the properties of the attracting regions. However, these diagrams have a major limitation since corresponding to only fixed values of the parameter  $e$ . For eliminating this handicap we can classify initial conditions in a new type of a 2D plane. The most interesting case corresponds to  $x = y$ , while the value of  $e$  will vary in the interval  $(0, 0.3125)$ . In this new 2D plane the coordinate  $x$  or  $y$  will be the abscissa, while the value of  $e$  will always be the ordinate. In part (a) of Figure 11 we depict the BOC on the  $(x = y, e)$  plane, while the corresponding distribution of the required iterations is given in part (b) of Figure 11. Inspecting carefully panel (a) we can clearly determine how the convergence properties evolve as a function of the  $e$ . Here, we would like to point out that the variable parameter  $e$  strongly affects the dynamics and the convergence properties of the system. This is very natural since the points of equilibrium (which control the dynamics of the system) are also directly affected by the parameter  $e$ .

The histograms shown in Figures 7-10 can be used as sources for additional information, about the

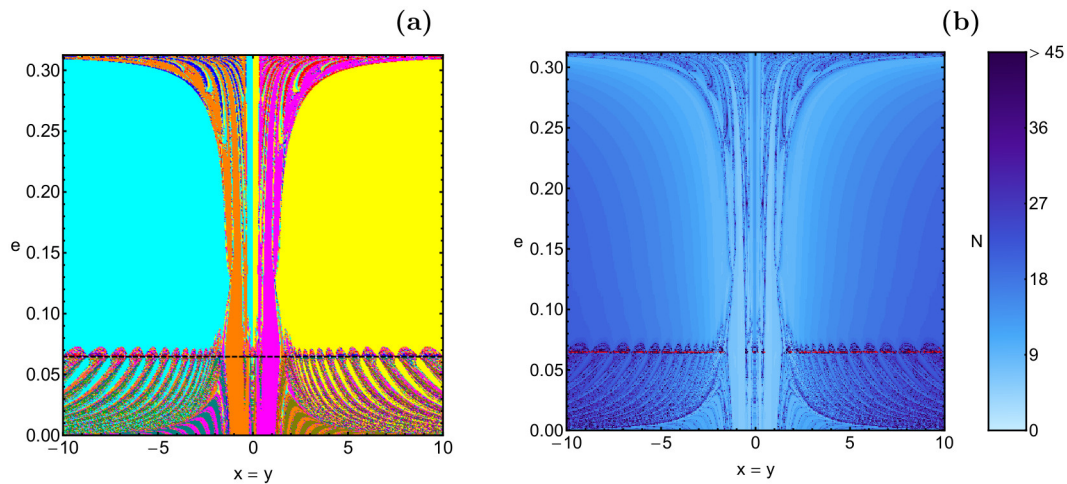


**Figure 11.** (a-left): The NR BOC on the  $(x = y, e)$  plane, when  $e \in (0, 0.3125)$ . The colors are the same as in Figs. 5 and 8. The horizontal, dashed black, line indicates the critical level  $e = e^*$ . (b-right): Distributions of the corresponding required numbers of iterations. (Color figure online).

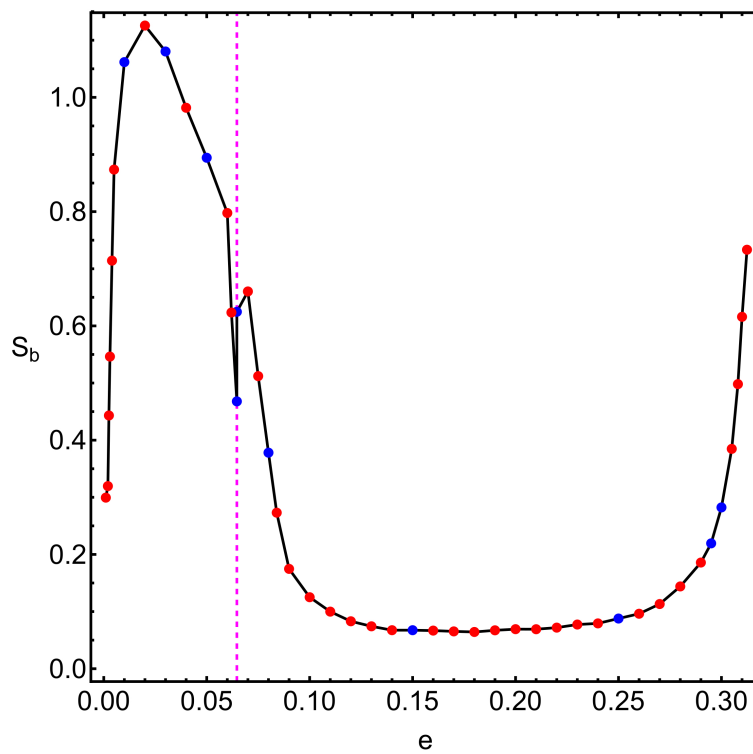


**Figure 12.** The entropy of the basins  $S_b$ , of the plane  $(x, y)$ , as a function of  $e$ . The vertical, magenta, dashed, line indicates the critical level of  $e$ . (Color figure online).

NR scheme. As an example, the right-hand side of the probability histograms can be fitted using the Laplace distribution. In Table 1 we provide the statistical information for the cases which were discussed earlier in Figs. 7 and 10. It is seen, that generally speaking  $l$  (the location parameter of the Laplace PDF) is relatively close to the average required number  $N$  of iterations (we have that  $|l - \langle N \rangle| \leq 1$ ). From this fact we can conclude that the Laplace PDF is an excellent fit for the

probability histograms of the NR scheme.

**Table 1.** Statistical information regarding the histograms presented in Figs. 7, and 10. The parameters  $l$  and  $d$  are the location parameter and the diversity which both enter the Laplace PDF.

Figure	$e$	$N^*$	$l$	$d$
7a	0.01	9	$N^* + 10$	8.2405
7b	0.03	18	$N^* + 1$	5.7692
7c	0.05	17	$N^* + 1$	4.7946
7d	0.064649	17	$N^* + 1$	5.1947

The fractal degree of a system can be quantitatively measured by calculating the quantity known as basin entropy  $S_b$  (Daza et al. (2016)). This tool compute the fractality of a basin entropy by examining its topological properties. The evolution of  $S_b$ , as a function of  $e$ , is depicted in Figure 12. Obviously, for creating the diagram shown in Figure 12 we used additional information (red dots) from other values of  $e$ , apart from those presented in Figs. 5 and 8 (blue dots).

Form the diagram of Figure 12 we can deduce that:

- When  $0 < e < 0.02$  the basin entropy increases sharply.
- When  $0.02 < e < e^*$  the basin entropy decreases rapidly.
- When  $0.07 < e < 0.14$  the basin entropy decreases.
- When  $0.14 < e < 0.25$  the basin entropy remains almost unperturbed.
- When  $0.25 < e < 0.3125$  the basin entropy increases.

It is interesting to note that two local minima of the basin entropy occur when the value of  $e$  tends to zero and also exactly at the critical value of  $e$ .

## 5. Conclusions

In this work we investigated the convergence properties and dynamics of the collinear restricted problem with three primaries and with a Manev-type potential. By integrating large sets of initial conditions we obtained the NR BOC, by means of basin diagrams with a color code. Additionally, we explored how the parameter  $e$  influences the convergence properties of the system. For measuring the level (degree) of fractality of the basin diagrams we calculated the respective basin entropy.

The most valuable conclusions are:

- (1) The analysis regarding the linear stability suggests that the points of equilibrium  $L_3$  and  $L_4$  are always linearly stable, while the libration points  $L_1, L_2, L_5, L_6, L_8$ , and  $L_9$  are always linearly unstable, when  $e \in (0, 0.3125)$ . On the other hand, the points  $L_7$  and  $L_{10}$  change from linearly unstable to linearly stable, when  $e > 0.30443155$ .

- (2) The NR BOC, corresponding to all points of equilibrium, extend to infinity, for all the permissible values of  $e$ . Moreover, the lines  $x = 0$  and  $y = 0$  are in fact axes of symmetry of the convergence areas on the configuration  $(x, y)$  plane.
- (3) Just above the critical level  $e^*$  we detected the presence of a portion of starting points that do not converge. Additional computations showed that these nodes do eventually converge to points  $L_1$  and  $L_6$  but only after a huge number of iterations ( $N \gg 500$ ).
- (4) Our thorough analysis of the nodes in all 2D types of planes did not report any valid non-converging starting points.
- (5) According to the evolution of the basin entropy, our system displays its highest degree of fractality around  $e = 0.02$ , while the lowest degree of fractalization was measured in the interval  $0.14 < e < 0.25$ . At the critical level,  $e^*$  the basin entropy exhibits a local minimum, thus suggesting that the properties of the system under consideration changes.

The routine of the multivariate NR scheme was coded in FORTRAN 77 (e.g., see Press et al. (1992)). For classifying the starting points on the configuration space, we needed, per grid, roughly about 3 minutes using a Quad-Core i7 4.0 GHz CPU. All the plots of the paper have been developed by using Mathematica<sup>®</sup> (Wolfram (2003)).

### ***Acknowledgment:***

*Our thanks go to Dr. Christof Jung for his valuable input.*

## **REFERENCES**

- Aguirre, J., Vallejo, J.C. and Sanjuán, M.A.F. (2001). Wada basins and chaotic invariant sets in the Hénon-Heiles system, *Phys. Rev. E*, Vol. 64, 066208.
- Aguirre, J., Viana, R.L. and Sanjuán, M.A.F. (2009). Fractal structures in nonlinear dynamics, *Rev. Mod. Phys.*, Vol. 81, pp. 333-386.
- Alavi, M. and Razmi, H. (2015). On the tidal evolution and tails formation of disc galaxies, *Astrophys. Space Sci.*, Vol. 360, 26.
- Alvarez-Ramirez, M., Barrabés, E., Medinaa, M. and Ollé, M. (2019). Ejection-Collision orbits in the symmetric collinear four-body problem, *Communications in Nonlinear Science and Numerical Simulation*, Vol. 71, 15.
- Arribas, M., Abad, A., Elipe, A. and Palacios, M. (2016a). Equilibria of the symmetric collinear restricted four-body problem with radiation pressure, *Astrophys. Space Sci.*, Vol. 361, 84.
- Arribas, M., Abad, A., Elipe, A. and Palacios, M. (2016b). Out-of-plane equilibria in the symmetric collinear restricted four-body problem with radiation pressure, *Astrophys. Space Sci.*, Vol. 361, 270.
- Barrabés, E., Cors, J.M. and Vidal, C. (2017). Spatial collinear restricted four-body problem with repulsive Manev potential, *Celest. Mech. Dyn. Astron.*, Vol. 129, pp. 153-176.

- Daza, A., Wagemakers, A., Georgeot, B., Guéry-Odelin, D. and Sanjuán, M.A.F. (2016). Basin entropy: a new tool to analyze uncertainty in dynamical systems, *Scientific Reports*, Vol. 6, 31416.
- Fakis, D.Gn. and Kalvouridis, T.J. (2013). Dynamics of a small body in a Maxwell ring-type  $N$ -body system with a spheroid central body, *Celest. Mech. Dyn. Astron.*, Vol. 116, pp. 229-240.
- Fakis, D.Gn. and Kalvouridis, T.J. (2014). On a property of the zero-velocity curves in the regular polygon problem of  $N + 1$  bodies with a quasi-homogeneous potential, *Rom. Astron. J.*, Vol. 24, pp. 7-26.
- Fakis, D.Gn. and Kalvouridis, T.J. (2017). The Copenhagen problem with a quasi-homogeneous potential, *Astrophys. Space Sci.*, Vol. 362, 102.
- Manev, G. (1924). La gravitation et le principe de l'action et de la réaction, *C.R. Acad. Sci. Paris*, Vol. 178, pp. 2159-2161.
- Manev, G. (1925). Die gravitation und das prinzip von wirkung und gegenwirkung, *Z. Phys.*, Vol. 31, pp. 786-802.
- Manev, G. (1930). Le principe de la moindre action et la gravitation, *C.R. Acad. Sci. Paris*, Vol. 190, pp. 963-965.
- Manev, G. (1930). La gravitation et l'énergie au zéro, *C.R. Acad. Sci. Paris*, Vol. 190, pp. 1374-1377.
- Mioc, V. and Stoica, C. (1997). On the Manev-type two-body problem, *Balt. Astron.*, Vol. 6, pp. 637-650.
- Moulton, F.R. (1910). The straight line solutions of the problem of  $N$ -bodies, *Annals of Mathematics*, Vol. 12, pp. 1-17.
- Nagler, J. (2004). Crash test for the Copenhagen problem, *Phys. Rev. E*, Vol. 69, 066218.
- Nagler, J. (2005). Crash test for the restricted three-body problem, *Phys. Rev. E*, Vol. 71, 026227.
- Palacios, M., Arribas, M., Abad, A. and Elipe, A. (2019). Symmetric periodic orbits in the Moulton-Copenhagen problem, *Celest. Mech. Dyn. Astron.*, Vol. 131, 16.
- Papadakis, K.E. (2007). Asymptotic orbits in the restricted four-body problem, *Planetary and Space Science*, Vol. 55, pp. 1368-1379.
- Press, H.P., Teukolsky, S.A., Vetterling, W.T. and Flannery, B.P. (1992). *Numerical Recipes in FORTRAN 77*, 2nd Ed., Cambridge Univ. Press, Cambridge, USA.
- Suraj, M.S., Asique, M.C., Prasad, U., Hassan, M.R. and Shalini, K. (2017). Fractal basins of attraction in the restricted four-body problem when the primaries are triaxial rigid bodies, *Astrophys. Space Sci.*, Vol. 362, 211.
- Suraj, M.S., Mittal, A., Kaur, C. and Aggarwal, R. (2018a). On the existence of libration points in the spatial collinear restricted four-body problem within frame of repulsive Manev potential and variable mass, *Chaos, Solitons and Fractals*, Vol. 117, pp. 94-104.
- Suraj, M.S., Zotos, E.E., Kaur, C., Aggarwal, R. and Mittal, A. (2018b). Fractal basins of convergence of libration points in the planar Copenhagen problem with a repulsive quasi-homogeneous Manev-type potential, *International Journal of Non-Linear Mechanics*, Vol. 103, pp. 113-127.
- Suraj, M.S., Abouelmagd, E.I., Aggarwal, R. and Mittal, A. (2019a). The analysis of restricted five-body problem within frame of variable mass, *New Astronomy*, Vol. 70, pp. 12-21.

- Suraj, M.S., Sachan, P., Zotos, E.E., Mittal, A. and Aggarwal, R. (2019b). On the fractal basins of convergence of the libration points in the axisymmetric five-body problem: The convex configuration, *International Journal of Non-Linear Mechanics*, Vol. 109, pp. 80-106.
- Suraj, M.S., Sachan, P., Zotos, E.E., Mittal, A. and Aggarwal, R. (2019c). On the fractal basins of convergence of the libration points in the axisymmetric five-body problem: The concave configuration, *International Journal of Non-Linear Mechanics*, Vol. 112, pp. 25-47.
- Suraj, M.S., Aggarwal, R., Mittal, A., Asique, Md.C. and Sachan, P. (2019d). On the perturbed photogravitational restricted five-body problem: the analysis of fractal basins of convergence, *Astrophys. Space Science*, Vol. 364, 87.
- Suraj, M.S., Zotos, E.E., Aggarwal, R. and Mittal, A. (2019e). Unveiling the basins of convergence in the pseudo-Newtonian planar circular restricted four-body problem, *New Astronomy*, Vol. 6, pp. 52-67.
- Wolfram, S. (2003). *The Mathematica Book*, Fifth Edition, Wolfram Media, Champaign.
- Zotos, E.E. (2016). Fractal basins of attraction in the planar circular restricted three-body problem with oblateness and radiation pressure, *Astrophys. Space Sci.*, Vol. 361, 181.
- Zotos, E.E. (2017a). Revealing the basins of convergence in the planar equilateral restricted four-body problem, *Astrophys. Space Sci.*, Vol. 362, 2.
- Zotos, E.E. (2017b). Equilibrium points and basins of convergence in the linear restricted four-body problem with angular velocity, *Chaos, Solitons & Fractals*, Vol. 101, pp. 8-19.
- Zotos, E.E. (2017c). Basins of convergence of equilibrium points in the pseudo-Newtonian planar circular restricted three-body problem, *Astrophys. Space Sci.*, Vol. 362, 195.
- Zotos, E.E. (2017d). Basins of convergence of equilibrium points in the generalized hill problem, *International Journal of Bifurcation and Chaos*, Vol. 27, 1730043-2193.
- Zotos, E.E. and Suraj, M.S. (2017). Basins of attraction of equilibrium points in the planar circular restricted five-body problem, *Astrophys. Space. Sci.*, Vol. 363, 20.
- Zotos, E.E., Satya, S.K., Aggarwal, R. and Suraj, M.S. (2018a) Basins of convergence in the circular Sitnikov four-body problem with nonspherical primaries, *International Journal of Bifurcation and Chaos*, Vol. 28, 1830016-386.
- Zotos, E.E., Suraj, M.S. Aggarwal, R. and Satya, S.K. (2018b). Investigating the basins of convergence in the circular Sitnikov three-body problem with non-spherical primaries, *Few-Body Systems*, Vol. 59, Article id. 69, 16 pp.
- Zotos, E.E., Suraj, M.S. Jain, M. and Aggarwal, R. (2018c). Revealing the Newton-Raphson basins of convergence in the circular pseudo-Newtonian Sitnikov problem, *International Journal of Non-Linear Mechanics*, Vol. 105, pp. 43-54.